Nanostructure of Nafion membrane material as a function of mechanical load studied by SAXS

Veroni Barbi[1], Sérgio S. Funari[2], Rainer Gehrke[3], Nico Scharnagl[4], Norbert Stribeck[1]*

[1]*Institute of Technical and Macromolecular Chemistry, University of Hamburg, Bundesstr. 45, 20146 Hamburg, Germany*
[2]*Max–Planck–Institute of Colloids and Interfaces, c/o HASYLAB at DESY, Notkestr. 85, 22603 Hamburg, Germany*
[3]*HASYLAB at DESY, Notkestr. 85, 22603 Hamburg, Germany*
[4]*GKSS Research Center, Postfach 1160, 21494 Geesthacht, Germany*

Received 27 January 2003; received in revised form 14 May 2003; accepted 30 May 2003

Abstract

The nanostructure of a perfluorinated membrane material (Nafion 117 by DuPont) is investigated as a function of strain and load by small–angle X–ray scattering (SAXS) at a synchrotron source. Two–dimensional SAXS patterns are evaluated utilizing the multi–dimensional chord distribution function (CDF). Anisotropy of the extruded material is considered. Both the ionomer domain and matrix polymer nanostructure are studied. For the neat material the classical ionomer domain model (domains as inverted micellae interconnected by channels) is confirmed and refined. Matching the plastic deformation behavior of the material, the domain structure in the relaxed and in the elongated state are found to be very similar.

During elongation, ionomer channels open to form hollow ionomer layers ("slits") that are oriented parallel to the strain with a thickness of 1.9 nm and a long period of 3.8 nm. The slit height increases from 3 nm at elongation $\varepsilon = 0.5$ to 6 nm at $\varepsilon = 1.25$, whereas the slit width decreases to 1.5 nm. The ultimate structure is characterized by ensembles of not more than three slits that are in good lateral register.

In the polymer matrix during elongation, cylindrical crystallites with a thickness of 2.5 nm and a most probable height of 7 nm are disrupted and parallelized with respect to the straining direction. The ultimate structure before sample failure is characterized by a broad domain height distribution ranging from a most probable domain height of 4 nm with a corresponding ultimate inclination of 40° to some perfectly parallelized domains of 20 nm height.

Keywords: Nafion, SAXS, plastic deformation

1 Introduction

Studies of structures and properties of perfluorinated ionomer membranes are numerous [1] and the corresponding interest is high because of the materials potential for proton exchange purposes. Even if only the papers on the finished commercial membranes Nafion® 117 and Nafion® 115 by DuPont Inc. are considered, a multitude of findings is reported. The findings are inconsistent in part. Using the novel method of multi-dimensional chord-distribution function (CDF) analysis we now present a study of the nanometer–scale morphology carried out by means of small–angle X–ray scattering using synchrotron radiation and compare our results to those of other groups.

CDFs computed from anisotropic scattering patterns visualize the multiphase nanostructure information in direct space. The interpretation of a CDF is straightforward, since it has been defined [2] by the Laplacian of Vonk's multidimensional correlation function [3]. Scattering patterns computed from simple model nanostructures (uncorrelated particles, microfibrils, lamellar stacks) yield the expected CDFs [2]. The CDF method has successfully been applied to the analysis of oriented semicrystalline polymers [4] and various thermoplastic elastomers studied during straining experiments [5–8]. In the earlier studies it has been compared to the classical method (discussion of peak position and shape as a function of strain or temperature).

Nafion® 117 and Nafion® 115 have frequently been

*Corresponding author. Tel.: +49-40-42838-3615; fax: +49-40-42838-6008. E-mail address: Norbert.Stribeck@desy.de

used for scattering studies. The difference is the thickness of 0.007 inches and 0.005 inches, respectively. In the majority of cases one–dimensional (1D) scattering curves are recorded and interpreted, although the material is anisotropic from the film extrusion process. Elliot et. al [9] were the first to report the considerable anisotropy of the scattering pattern from neat Nafion® 115 and Nafion® 117. When strained in machine direction (MD) or transverse direction (TD), respectively, the authors report that the material keeps showing different scattering patterns. On a conventional X–ray source they record a scattering pattern of 8 bit depth in 24 h. Because of this low scattering power, synchrotron radiation is required to collect high quality data in reasonable time.

The complexity of the scattering pattern of Nafion® 117 has been observed early. In addition to a common small–angle X–ray scattering (SAXS) peak, the material exhibits a strong peak at a scattering angle of 2.7^{o} (middle–angle X–ray scattering (MAXS)). In 1981 Fujimori et al. [10] have explained the SAXS peak from the semicrystalline structure of the fluorinated polymer and the MAXS peak from the preferential distance among ionic microdomains. In the sequel, size and arrangement of the microdomains are studied by several groups [11–13]. Lee et al. [14] melt and quench the membrane. This way they obtain an amorphous material that shows the MAXS only. They vary the contrast and use neutron scattering to record scattering curves. After Fourier inversion they obtain radial distribution functions. A model of spheres in a matrix is fitted to the data. The fit results in a microdomain diameter of 1.85 nm and an average distance of 7 nm among them. From the water uptake of the membrane they conclude that the ionic microdomains have to be interconnected by channels that cannot be detected in the scattering data. The finding is explained, if the channels and the microdomains are lined with an interfacial layer of an electron density close to that of the fluoropolymer. Thin channels in this case are filled by the interfacial layer and their scattering effect is very low. Thus the authors support the domain–channel model proposed by Gierke and Hsu [15, 16] and reviewed by Heitner–Wirgun [1].

More recent papers have been published by several groups [17–21]. Gebel and Lambard [17] collect scattering curves of Nafion® 117 over a wide angular range and test the applicability of various models by comparing the fit quality when applied to the curves. They find that an appropriate model has to consider the arrangement of the ionic microdomains but that, in agreement with Lee et al. [14], the consideration of the interfacial layer does not improve the quality of the fit. They report a microdomain radius of 1.98 nm and an average microdomain distance of 4.22 nm. Haubold et al. [20] fit a 1D scattering curve in a double–logarithmic representation to a sophisticated microstructural model: A column extruded from a rectangular base and sawn through in the middle to yield a gap making the ionic microdomain. For the dry Nafion 117 they report a gap width of 2 nm and a total sandwich height of 8 nm. Matsuyama et al. [18] report that they cannot find the MAXS scattering of Nafion® 117. Kreuer [19] finds it. Kim, Kim and Jung [21] propose a macrolattice made from cylindrical microdomains based the observation of two broad SAXS scattering peaks in a curve from Nafion® 117. Rubatat et al. [22] suggest a new structural model ("polymeric bundles") based on small–angle neutron scattering (SANS) and SAXS measurements evaluated by models developed for isotropic scattering data. Additionally, they present data from a synchrotron microfocus experiment that confirms and extends the anisotropy earlier reported by Elliot et. al [9]. According to their findings the machine direction (MD) of Nafion® 117 is not a perfect axis of symmetry, insofar they even observe some anisotropy in the 2D scattering patterns when the material is rotated about MD.

2 Experimental

2.1 Material

Nafion® 117 extruded film (equivalent weight 1100 g, thickness 0.007 inches (0.177 mm)) was obtained from Ion Power Inc., Bear, DE, USA.

2.2 SAXS and straining

SAXS experiments were performed in the synchrotron beam line A2 at HASYLAB, Hamburg, Germany. The wavelength of the X-ray beam was 0.15 nm. SAXS images were collected by a two–dimensional position sensitive CCD detector (MAR 185®; 2048×2048 pixels of $0.079 \times 0.079\,\mathrm{mm}^2$ binned to 1024×1024 pixels). Two different setups with sample–to–detector distances of 1620 mm and 1020 mm were required in order to record both the central portion of the scattering pattern (small–angle X–ray scattering, SAXS) and the outer part (middle–angle X–ray scattering, MAXS) with sufficient accuracy. The minimal accessible scattering angle corresponded to a d–spacing of 33 nm. The maximal scattering angle corresponded to 1.8 nm. The flux of the attenuated primary beam was measured using a pin diode in the beam stop. Rectangular sample strips ($40 \times 12\,\mathrm{mm}^2$) with elongational marks were mounted in a straining stage (courtesy of B. Heise, University of Ulm, Germany), positioned in the synchrotron beam and irradiated in the normal direction (ND) of the extruded membrane. Specimens were slowly (5 mm/min) strained up to a chosen true elongation and exposed for 2 to 6 min (approx. 5000 counts accumulated in the SAXS peak maximum). After each measurement in elongation the samples were unloaded, exposed in the relaxed state, and strained to the next elongational level. These cycles were repeated until failure of the sample in steps of $\Delta\varepsilon = 0.25$ with the elongation defined by $\varepsilon = \left(\ell - \ell_0\right)/\ell_0$; ℓ and ℓ_0 being the actual

and the initial length, respectively, as measured between two marks on the sample enclosing the irradiated volume.

3 Data evaluation

We did not evaluate the 2D data by extracting scattering curves and fitting them using models valid for isotropic data, nor did we perform a full 3D analysis. Instead, because of the limitations of our instrument, we assumed fiber symmetry (about MD) and thus disregarded the slight additional anisotropy that had been demonstrated by rotating Nafion film about MD in a synchrotron microfocus beam [22].

2D scattering patterns were normalized with respect to the incident flux and blind areas were masked. The instrument background was subtracted considering sample absorption as measured by a pin–diode in the beamstop. Center and orientation of the patterns were determined. The patterns were aligned and averaged with respect to the four quadrants. Remnant blind spots were filled utilizing a two-dimensional extrapolation based on radial basis functions [23]. The same extrapolation method was applied to define a smooth continuation of the measured data up to $-0.8\,\mathrm{nm}^{-1} < s_{12}, s_3 < 0.8\,\mathrm{nm}^{-1}$. Characteristic for Nafion is the observation both of common SAXS ("matrix peaks" [22]) and a scattering at a higher scattering angle (medium-angle X-ray scattering, MAXS; "ionomer peaks" [22]). The structures related to these two effects can be separated by application of different spatial frequency filters to the scattering patterns.

Data processing was performed similar to the procedure described in earlier work [2]. The samples exhibiting discrete and anisotropic scattering were processed to yield the 2D chord distribution, $z\left(r_{12}, r_3\right)$, with cylindrical symmetry. The positions of maxima and minima in $z\left(r_{12}, r_3\right)$ were determined. Based on these data conclusions on the nanostructure were drawn.

In detail, the preprocessed anisotropic images were projected onto the fiber plane and multiplied by s^2 (i.e. application of the Laplacian in reciprocal space [2]) resulting in $s^2\{I\}_2\left(s_{12}, s_3\right)$. Here $\mathbf{s} = \left(s_{12}, s_3\right)$ is the scattering vector in cylindrical co–ordinates with its modulus $|\mathbf{s}| = s = (2/\lambda)\sin\theta$, λ the wavelength of X–radiation, and 2θ the scattering angle. It must be stressed that the computation of the CDF does not involve noise filtering. Instead, the projection that is required due to the Fourier slice theorem [2, 24, 25] diminishes the noise. By projecting the data we do not eliminate information, but preserve it.

After multiplication by s^2, the "ionomer structure" is the predominant one. As compared to the "matrix structure" it is related to relatively low spatial frequencies from the scattering pattern that are close to the spatial frequencies of the diffuse SAXS background. Cautious background subtraction by single–step spatial frequency filtering preserves the information on the ionomer structure. Background elimination by iterated filtering considers even the ionomer peaks a background and ends with a function describing the "matrix structure". Single–step application of the spatial filtering procedure [2] to $s^2\{I\}_2\left(s_{12}, s_3\right)$ resulted in the interference function, $G_{2,I}\left(s_{12}, s_3\right)$, of the ionomer structure. The iterative spatial frequency filter resulted in the interference function, $G_{2,M}\left(s_{12}, s_3\right)$, of the semicrystalline polymer matrix. These functions finally were subjected to a 2D Fourier transformation, resulting in multidimensional chord distribution functions (CDFs) of the nanostructure. The interpretation of such functions is straightforward, since the CDF has been defined [2] by the Laplacian of Vonk's multidimensional correlation function [3]. As such it presents the autocorrelation of the surfaces from the (nanosize) domains in space in a similar manner as Ruland's interface distribution function does [26–28] for one–dimensional structures as a function of distance. For samples with fiber symmetry the CDF $z\left(r_{12}, r_3\right)$ is a function of two co-ordinates only (transverse direction r_{12} and fiber direction r_3). It can thus completely be visualized by surface plots, density plots or contours in a plane. Positive peaks found in the vicinity of the origin are size distributions of the primary domains. Thus their size, shape and orientation in space are depicted. Negative peaks following farther out exhibit "long periods", i.e. the distance of two adjacent domains from each other. Positive peaks following next describe the size and orientation of superdomains (i.e. clusters made from two adjacent domains), and correlations among domains more distant are manifested in consecutive peaks at even longer distance.

It must be stressed that the CDF is not the famous chord distribution curve $g(r)$ of isotropic materials [29–32], the interpretation of which is much more difficult than the interpretation of the CDF, because in $g(r)$ the information on the nanostructure is subjected to solid sphere average. In our CDFs this information is only subjected to azimuthal average, and thus the peaks are found in a plane of direct space, not in a curve.

4 Results and discussion

4.1 Scattering patterns

Fig. 1 shows scattering patterns of Nafion® 117 in different stages of the straining experiment. All patterns show a typical small–angle X–ray scattering (SAXS) in the center ("matrix peak") and a strong medium–angle scattering (MAXS) ("ionomer peak") which is partially truncated due to the long sample–to–detector distance (1620 mm) chosen here in order to ensure that no SAXS features are truncated by the beam stop in the center.

As has been found by others [9, 22], the neat material shows an elliptical SAXS peak of almost constant intensity. The maximum in MD corresponds to 15.4 nm. The maximum in TD corresponds to 13.1 nm. The MAXS ionomer

peak, on the other hand, has a circular shape (radius corresponding to 3.2 nm) with an intensity modulation. Its maximum is perpendicular to MD.

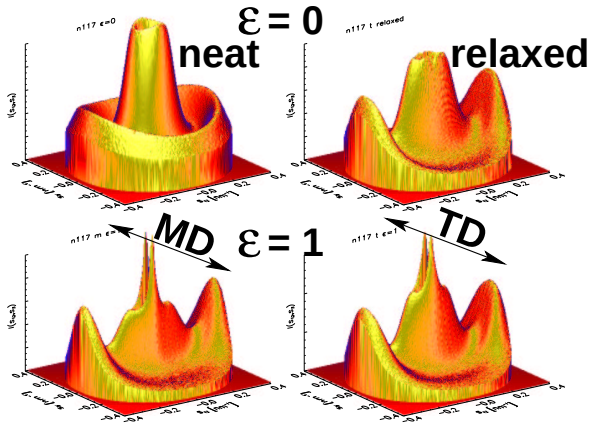

Figure 1: Dry Nafion® 117 film. SAXS intensity $I\left(s_{12},s_3\right)$, ($-0.4\,\mathrm{nm}^{-1} \leq s_{12},s_3 \leq 0.4\,\mathrm{nm}^{-1}$; long sample–to–detector distance) before, during and after straining to $\varepsilon = 1$. Bottom left: Strained in machine direction (MD). Bottom right: strained in transverse direction (TD).

Straining in MD and TD, respectively, results in similar but not identical scattering patterns. At an elongation of $\varepsilon = 1$ both the recorded patterns show a ionomer peak with maxima on the equator corresponding to a d–spacing of 2.9 nm. The elliptical SAXS peak in the center is converted to diamond shape with pointed maxima on the meridian. Its positions correspond to a long period of 38 nm. These pointed features can only be observed in the strained state. After relaxation from $\varepsilon = 1$, we now find a small dent at the meridian (long period now: 33 nm), whereas the long period on the equator (13.1 nm) and the position of the ionomer peek keep constant upon relaxation. This finding corresponds to the macroscopic observation that the deformation is predominantly plastic.

4.2 Chord distributions of the ionomer structure

Fig. 2 shows the projected scattering intensity $\{I\}_2\left(s_{12},s_3\right) = \int I\left(s_1,s_2,s_3\right) ds_2$ of neat Nafion® 117, now from the straining experiment with the shorter distance of the detector.

In the center the ellipsoidal, isointensity SAXS peak is detected. Farther out the circular ionomer reflection with peak maxima on the equator (s_{12}–direction) is found. With respect to the membrane extrusion process the equator is the TD, and the meridian the MD, respectively. Part of the extrapolated apron shows up in the corners of the displayed window.

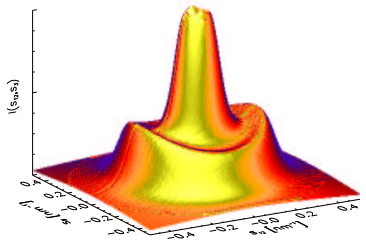

Figure 2: Neat Nafion® 117. Scattering intensity $\{I\}_2\left(s_{12},s_3\right)$ projected onto the representative plane with the fiber axis chosen in MD. Visible range: $-0.5\,\mathrm{nm}^{-1} \leq s_{12},s_3 \leq 0.5\,\mathrm{nm}^{-1}$.

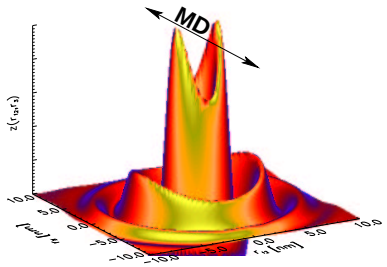

Figure 3: Multidimensional chord distribution function (CDF) $z_M\left(r_{12},r_3\right)$ of the MAXS structure, (-10 nm $\leq r_{12},r_3 \leq$ 10 nm) of Nafion 117® as extruded (domain peaks). Machine direction(MD, r_3) is indicated by an arrow.

From $s^2\{I\}_2\left(s_{12},s_3\right)$ the interference function of the ionomer structure, $G_{2,I}\left(s_{12},s_3\right)$ is computed by single–step spatial frequency filtering. After 2D Fourier inversion of $G_{2,I}\left(s_{12},s_3\right)$ the chord distribution function (CDF) of the ionomer structure is retrieved. Fig. 3 shows the CDF of the neat material seen from the top. The elevated peaks seen here are related to the domains of the nanostructure.

The function demonstrates the correlations among domain surfaces. It fades away in a cylindrical region of ± 10 nm that is typical for the correlation among surfaces of ionomer domains. The central ring is related to the autocorrelation of the basic ionomer domain. Its radius is a measure of their average size. The observed value of 1.9 nm is in good agreement with the finding of Lee et al. [14], but much smaller than the value originally estimated by Hsu and Gierke [16] on the basis of water uptake. The intensity of the ring is modulated considerably. This means that the ionomer domains cannot be spheres. Instead, the area of contact between the domain and its ghost is larger if the ghost is shifted by 1.9 nm in equatorial direction than if it is shifted by the same amount in meridional direction. Thus for the ionomer domains in the neat material we find both preferential orientation and some anisotropy (the domains are oblate with respect to the TD). The CDF exhibits that a scattering effect of channels connecting the ionomer domains cannot be observed. This is in good agreement with

the results of fit–model variation presented by several authors [14, 17, 20].

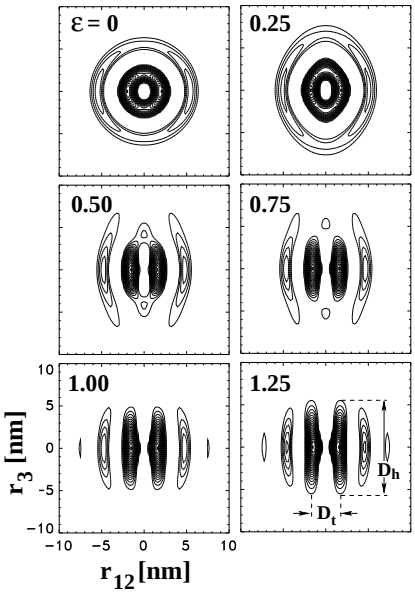

Figure 4: Strained Nafion® 117. Contours of the positive peaks (related to the domains) in the CDF $z_M\left(r_{12}, r_3\right)$ of the MAXS structure. Straining direction(r_3) is vertical. D_t: Average domain thickness. D_h: Maximum domain height

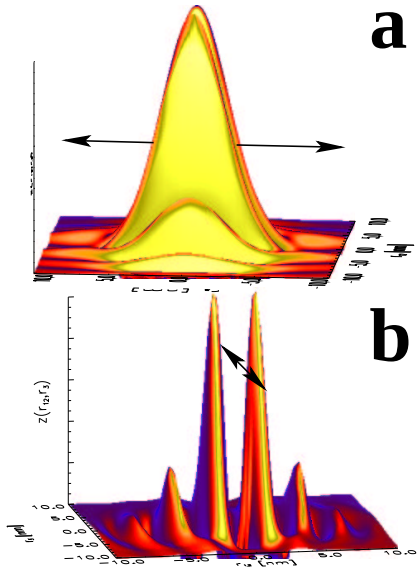

Figure 5: Nafion 117® at $\varepsilon = 1.25$. Domain dimension peaks from the CDF $z\left(r_{12}, r_3\right)$ viewed (a) perpendicular and (b) parallel to the straining direction, r_3, indicated by double head arrows.

Stretching the sample changes the nanostructure and thus the CDF. Fig. 4 shows the contours of the domain peaks in the CDF as a function of the elongation ε.

Indicated in the drawing is a method to determine the average domain height, D_t. It is applicable for elongations $\varepsilon \geq 0.5$. Beginning from this elongation the domain height, D_h, can be determined as well. The almost perfect triangular shape in meridional direction of the strong domain peaks (Fig. 5a) shows that the domain height distribution is rather narrow. Thus the height of the ionomer domain in the strained state is well defined.

In equatorial direction (Fig. 5b) the inner peaks are narrow. This means that even the thicknesses of the domains are well defined. Autocorrelation domain peaks on the meridian are not observed. Thus the ionomer domains in the strained state are no cylinders, but are readily described by slabs oriented parallel to the strain. We have found a similar arrangement of layers parallel to the straining direction in a recent study [6] on polyether-*block*-polyamides (PEBA) for a material with a nanostructure formed from lamellar domains ([6], 57PEO/PA6).

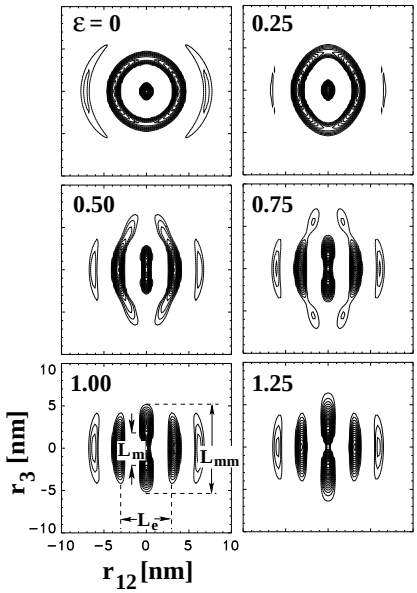

Figure 6: Strained Nafion 117®. Contours of the negative peaks (related to the long periods) in the CDF of the MAXS structure. Straining direction(r_3) is vertical. L_m: Most probable long period in meridional direction. L_{mm}: Maximum long period in meridional direction. L_e: Average long period in equatorial direction.

Information concerning the distances among the domains ("long periods") can be gathered from the negative peaks of the CDF (Fig. 6).

Indicated in the drawing is the determination of some characteristic parameters. L_m is the most probable long period between two domains arranged on top of each other in straining direction (forming a "nanofibril"). The distribution is extremely wide, and L_{mm} is characteristic for the maximum long period in straining direction. L_e specifies the distance in equatorial direction of two domains. It is obvious that in straining direction not more than two domains (or fragments) are poorly correlated, whereas in the transverse direction even the correlation with the second neighbor is still strong.

There are no significant differences concerning the

ionomer domain nanostructure between a straining in MD or TD, respectively. The relaxed structure is qualitatively equivalent to the structure that has been observed in the elongated state before.

Fig. 7 presents the parameters of the ionomer nanostructure extracted from the CDFs. The long period in equatorial direction, L_e, (open circles) is decreasing as a function of increasing strain from 3.8 nm at $\varepsilon = 0$ to 3.1 nm at $\varepsilon = 1.25$. This demonstrates the transverse contraction of the nanostructure. The average domain thickness, D_t, (filled circles) gives a constant value of 1.5 nm. In the observed domain thickness distribution (cf. Fig. 5b) information concerning the matrix and the ionomer domains, respectively, cannot be separated from each other because $L_e \approx 2D_t$ is valid. The domain height (D_h, filled diamonds) obviously is a linear function of the elongation ε. Extrapolation towards $\varepsilon = 0$ yields a value of $D_{h,0} = 1.9$ nm; and this value is identical to the average domain size extracted from the CDF domain peak of the neat material. It is noteworthy that the increase of D_h as a function of elongation is stronger than that expected for an affine deformation. The expected value at $\varepsilon = 1$ is 3.8 nm, but $D_{h,1} = 4.9$ nm is found. Such a strong increase can rather be explained by some kind of craze propagation process than by a common deformational process.

Resorting to the domain–channel model proposed by Gierke and Hsu [15, 16], the observed evolution of the ionomer nanostructure can be interpreted smoothly. The neat ionomer domains show a diameter of 1.9 nm. Their average distance is double this value (10% smaller than the long period found by Gebel and Lambard [17] in water–swollen Nafion® 117, but much lower than the value found by Lee et al. [14] in molten and quenched material). In the neat material the ionomer domains are connected by channels that are completely filled by the interphase liner and thus invisible to the SAXS. In the straining experiment the applied force widens the channels selectively, as a function of the angle between applied force and the direction of the channel. The observed slab–shaped domains are formed during the straining experiment by the merging of adjacent domains and widened channels into layer–shaped voids. We may address the resulting ionomer domains by naming them void–layers. A peculiar feature is the obvious self–organization of a set of adjacent void–layers in the course of the straining experiment. In a first step, ensembles of layers are formed with a stacking direction more or less perpendicular to the strain, which, in a second step, increase the perfection of orientation, distance and correlated domain height. Nevertheless, there is no stacking of such ensembles in the straining direction, and thus no formation of a smectic structure.

Admittedly, in the CDF on the meridian we observe a (very broad) distribution of long periods. Its upper limit, L_{mm}, (cf. Fig. 7) is not only a linear function of elongation ε, but even proportional to it. On the other hand, the relation $L_{mm}(\varepsilon) \approx D_h(\varepsilon)$ holds, and the most probable value of the meridional long period, L_m, is rather small. This findings can be explained in the simplest way by assuming struts, (i.e. "polymeric bundles" [22]), crossing the ionomeric void–layers at almost a random position. Then a sequence void–material–void is present in the straining direction that causes the observed and very broad long period peaks on the meridian of the CDF.

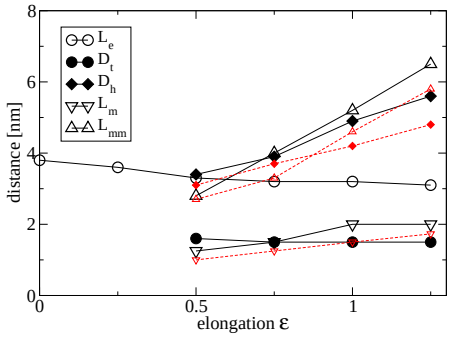

Figure 7: MAXS–related nanostructure of Nafion 117® in strained and relaxed state. Evaluation of the CDFs results in dimensions of the domains and the long periods as a function of elongation. Solid lines and large symbols: sample strained. Dashed lines and small symbols: sample after relaxation from strain. In equatorial direction changes upon strain are small and not shown here. L_e: long period in equatorial direction. D_t: domain thickness (equatorial direction). D_h: domain height. L_m: meridional long period, most probable value in straining direction. L_{mm}: meridional long period, maximum value.

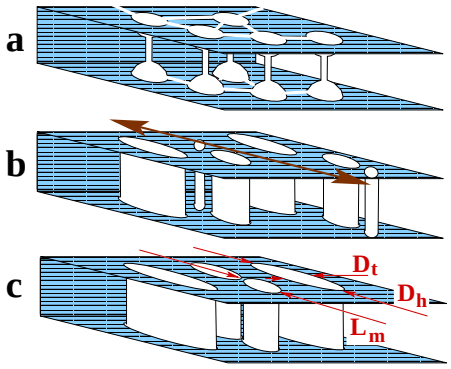

Figure 8: Sketch of a void–layer structure and its evolution during straining of Nafion 117® that is compatible with the nanostructure data extracted from the measured MAXS patterns. (a) native material. (b) medium elongation. The straining direction is indicated by a double arrow. (c) high elongation. The domain thickness, D_t, domain height, D_h, and the meridional long period of the CDF, L_m, that is resulting from struts crossing the void–layers.

Resuming, the structural notion resulting from the CDF analysis is sketched in Fig. 8. The neat Nafion® film (Fig. 8a) contains oblate ionomer domains with a diameter of 1.9 nanometer at an average distance of 3.8 nm from each other. These inverted micellae are connected by channels that are invisible to the X–ray method. During the straining experiment some of the channels widen and become visible. In such a way void–layers are formed (Fig. 8b,c). At

medium elongation (Fig. 8b) there are void–layers with uniform extension in straining direction that are not yet perfectly aligned. At the ultimate elongation (Fig. 8c) adjacent void–layers have aligned with respect to each other. The layers are intermitted by struts at more or less random position.

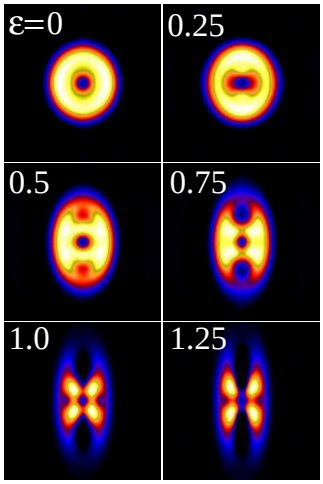

Figure 9: Nanostructure of the polymer matrix of Nafion® 117 during elongation (transverse to MD). CDFs $z\left(r_{12}, r_3\right)$, $-20\,\text{nm} \leq r_{12}, r_3 \leq 20\,\text{nm}$, (domain peaks) as a function of elongation ε.

4.3 The chord distributions of the polymer matrix

By iterative spatial frequency filtering the nanostructure of the perfluorinated matrix itself was extracted. Then the corresponding CDF was computed. The first step suppresses the information on the ionomer structure that initially was contained in the SAXS pattern, and we are viewing the nanostructure using a lower magnification. Fig. 9 exhibits the evolution of the matrix CDFs (domain peaks) during the straining of Nafion® 117 transverse to the machine direction of the commercial film. Low elongations show the inversion of the initial preferred orientation. Thereafter a four–point ensemble of domain peaks is emerging. Such CDF patterns indicate the presence of tilted cylindrical domains. The tilt angle between the straining direction and the cylinder axes is decreasing as a function of increasing elongation.

Fig. 10 demonstrates the differences of the matrix nanostructure that are observed when the material is strained in different directions with respect to the machine direction (MD) of the extruded film. The differences are small. Starting from an elongation $\varepsilon = 0.5$ the positions of the domain and long period peaks in the CDFs are identical, but the widths of the peaks are considerably wider when the material is strained in transverse direction (TD). From this finding it follows that the variation of cylinder heights and tilt angles is lower if Nafion 117 is strained in machine direction.

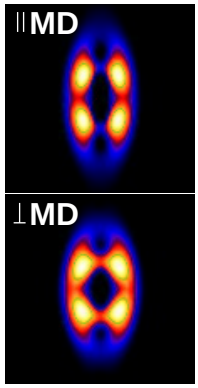

Figure 10: Different straining directions and the nanostructure of Nafion 117. The CDF domain peaks are shown at $\varepsilon = 1.0$. Straining direction is vertical. Narrow peaks (top) when straining in MD. Broader domain peaks (bottom) when straining in TD. Peak positions are identical.

Comparing the CDFs of the strained material to the ones of the relaxed material we find that the qualitative differences between both kinds of nanostructures are small, as expected for a material exhibiting a plastic deformation behavior rather than an elastic one. Even the positions of the domain and long period peaks are almost identical (Fig. 11).

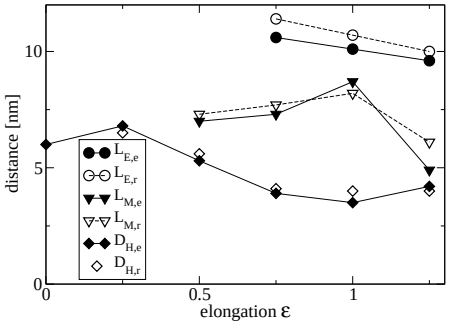

Figure 11: Comparing strained and relaxed state of the nanostructure of the polymer matrix of Nafion 117 as a function of elongation. Domain dimensions and long periods as evaluated from the CDFs. Filled symbols: sample strained. Open symbols: sample after relaxation from strain. L_E: Long period in equatorial direction (observed only at high elongation). L_M: Meridional long period (maximum of narrow peak). D_H: Most probable domain heights (in oblique direction).

Only the top pair of curves (i.e. the most probable long period in equatorial direction, L_E) shows a significant difference. In the relaxed state the lateral distance between neighboring cylinders is somewhat wider than in the strained state. As a function of increasing strain the lateral distance is decreasing from a value above 10 nm to a value below 10 nm. We would like to point out that the data in the figure do not reflect average values, but the most probable ones as given by the maxima of the corresponding domain size distributions. A more sophisticated method would have to separate the distributions from each other. Such method is not yet available.

The central pair of curves demonstrates the long period in straining direction, L_M. Up to an elongation of $\varepsilon = 1$ a moderate increase from 7 nm to 8 nm is observed. At $\varepsilon = 1.25$ failure of the material is signalized by a strong decrease of the long period that can be explained by disruption of domains.

The bottom pair of curves shows the most probable heights of the cylinders measured in the direction of their axes. There is no difference between elongated and relaxed state. The first value at $\varepsilon = 0$ is associated to a poorly oriented sample and thus is subjected to considerable averaging. Thereafter we observe a shift of the maximum of the domain peaks closer to the origin of the CDF (7 nm to 4 nm).

Associated with these oblique domains there are oblique long periods as well, but the corresponding peaks are broad and weak. Only at medium orientation the distance of the peak maximum from the origin of the CDF can be determined: 13.5 nm and 12.1 nm at $\varepsilon = 0.5$ and $\varepsilon = 0.75$, respectively. At higher elongations a weak long period ridge is running almost parallel to the equator, at lower elongations the anisotropy of the peaks is small and we observe a ring with long periods of 12.3 nm and 14.2 nm corresponding to elongations of $\varepsilon = 0$ and $\varepsilon = 0.25$, respectively.

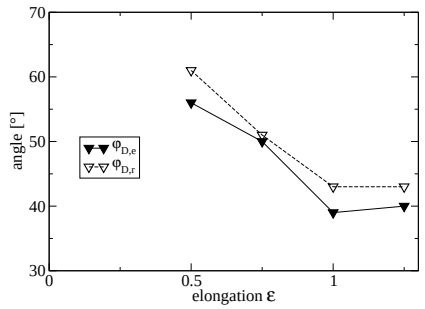

Figure 12: Domain orientation of the matrix–related nanostructure of Nafion 117® in strained (filled symbols) and relaxed state (open symbols) as evaluated from the CDFs. φ_D is the most probable angle enclosed by the straining direction and the axis of the cylindrical domains.

Summarizing the results we have found that the crystalline domains in the matrix are damaged by the straining process beginning from low elongations. If the material is strained to more than double the initial length, massive damage is observed which initiates the macroscopic failure of the membrane. A possible reason for the well–behaved nature of the material up to an elongation of $\varepsilon = 1$ can be deduced from a plot of the most probable tilt angle of the cylinders (Fig. 12).

Up to the critical elongation of $\varepsilon = 1$ the tilt angle of the domains decreases linearly and afterwards remains constant at 40°. Thus the well–behaved nature of the plastic deformation appears to be coupled to the ease of rotability of anisotropic crystalline domains in the matrix polymer.

4.4 The ultimate structure of the polymer matrix

Close to the macroscopic failure of the samples we observe the ultimate nanostructure of the polymer matrix. A contour plot of the domain peaks in the corresponding CDF is shown in Figure 13.

The contour plot demonstrates the complexity of the domain nanostructure in the matrix polymer of Nafion® 117.

Following the arrow in the figure down the domain peak we scan the ensemble of crystalline cylinders moving from the many, short (4 nm) and tilted (40°) ones to the few, hardly inclined and long (20 nm) cylinders. The width of the ridge (dashed lines) is almost constant and corresponds to an average cylinder diameter of 2.5 nm. Several possibilities of combining the ionomer and the matrix structures can be imagined. Because no evidence on the most favorable model can be extracted from the scattering data we refrain from speculation.

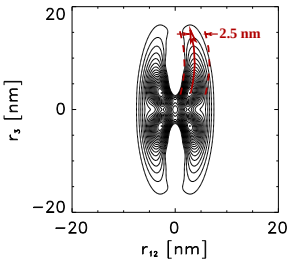

Figure 13: Ultimate nanostructure of the polymer matrix of Nafion® 117. Positive contours of the domain peaks from the CDF. Strained state at $\varepsilon = 1.25$. The arrow indicates the correlation between domain height and orientation, starting from short and poorly parallelized domains. Broken lines indicate the estimation of the almost constant domain diameters.

5 Conclusions

We have investigated the nanostructure evolution in the straining process of dry Nafion® 117 film by interpretation of the multidimensional chord distribution function (CDF). In analogy to common technology the CDF is associated to the virtual image that is observed when shining light on a holographic plate — and, correspondingly, the plate pattern itself is associated to the complete SAXS pattern in reciprocal space. In this context classical SAXS method resembles interpretation of the fringes in the hologram, whereas the CDF method is interpretation of the virtual image. Here, for the first time, we have studied nanostructures that are present in different “magnifications of the image”. With respect to the CDF method the change of magnification is proposed to be accomplished by changing the limiting frequency in a spatial frequency filter that is inherent to the CDF method.

The method itself takes advantage both of mathematical concepts developed several decades ago [3, 24–26], and of procedures developed in the field of digital image processing and computer tomography (CT) [33–36]. In fact, the computation of projection and Fourier inversion resembles the imaging procedure from the field of CT ("Fourier back projection"), and from this field concepts concerning stability and fidelity of the CDF image could be adopted and implemented in a joint effort of the community. As compared with the sophisticated data treatment from the field of CT, the presented state of SAXS data evaluation is still embryonic.

Finally we have to again stress that the CDF image is not a picture in the usual sense, but only shows the correlations among the domain surfaces in space. This information is not corrupted by the loss of phase information in the scattering process. Nevertheless, even the interpretation of these correlations in direct space is more adapted to human perception than is the interpretation of fringes in a scattering pattern.

According to our results the macroscopic plasticity of the material is generated, first, by weak spots (the postulated ionomer domain–channel network that, upon application of strain, is becoming visible in the CDF from the SAXS data), and second, by fragile anisotropic crystal domains that break and/or rotate upon application of mechanical load. In particular the response of the ionomer network upon mechanical load should result in a considerable change of the transport properties of the membrane.

In order to rule out the uncertainty resulting from the assumption of perfect fiber symmetry, much higher experimental and data evaluation effort would be required starting from series of scattering patterns recorded as a function of rotating angle about MD (and, of course, mechanical load status). Because of the low scattering power such an experiment would require an extremely high flux radiation source like a free electron laser (FEL). Then it would become possible to reconstruct the CDF in three dimensions and to describe the nanostructure of the membrane with respect to the three principal directions of the anisotropic film.

Acknowledgments. Support of this work by GKSS project 6.T3.00.G.01.–HS 1 and HASYLAB project II–01–041 is gratefully acknowledged.

References

[1] Heitner-Wirgun C. J Membr Sci 1996;120(1):1–33.
[2] Stribeck N. J Appl Cryst 2001;34(4):496–503.
[3] Vonk CG. Colloid Polym Sci 1979;257:1021–1032.
[4] Stribeck N, Bayer R, von Krosigk G, Gehrke R. Polymer 2002;43(13):3779–3784.
[5] Stribeck N, Fakirov S. Macromolecules 2001; 34(22):7758–7761.
[6] Barbi V, Funari SS, Gehrke R, Scharnagl N, Stribeck N. Macromolecules 2003;38(3):749–758.
[7] Stribeck N, Androsch R, Funari SS. Macromol Chem Phys 2003;in print.
[8] Stribeck N, Fakirov S, Apostolov AA, Denchev Z, Gehrke R. Macromol Chem Phys 2003;204(7):1000–1013.
[9] Elliott JA, Hanna S, Elliott AMS, Cooley GE. Macromolecules 2000;33(11):4161–4171.
[10] Fujimura M, Hashimoto T, Kawai H. Macromolecules 1981;14(5):1309–1315.
[11] Fujimura M, Hashimoto T, Kawai H. Macromolecules 1982;15(1):136–144.
[12] Wu DQ, Liang B, Hsiao BS, Li Y, Chu B. Polym Prepr Am Chem Soc Div Polym Chem 1992;33(1):350–351.
[13] Halim J, Büchi FN, Haas O, Stamm M, Scherer GG. Electrochim Acta 1994;39(8-9):1303–1307.
[14] Lee EM, Thomas RK, Burgess AN, Barnes DJ, Soper AK, Rennie AR. Macromolecules 1992;25(12):3106–3109.
[15] Gierke TD, Hsu WS. In: Eisenberg A, Yeager HL, editors, *Perfluorinated Ionomer Membranes*, number 180 in ACS Symp. Ser. Washington DC: American Chemical Society 1982; pp. 283–307.
[16] Hsu WY, Gierke TD. J Membr Sci 1983;13(3):307–326.
[17] Gebel G, Lambard J. Macromolecules 1997; 30(25):7914–7920.
[18] Matsuyama H, Kitamura Y, Doi Y, Ohtsuka S, Matsuba Y, Okihara T. J Appl Polym Sci 1999;73(6):961–968.
[19] Kreuer KD. J Membr Sci 2001;185(1):29–39.
[20] Haubold HG, Vad T, Jungbluth H, Hiller P. Electrochim Acta 2001;46(10-11):1559–1563.
[21] Kim J, Kim B, Jung B. J Membr Sci 2002;207(1):129–137.
[22] Rubatat L, Rollet AL, Gebel G, Diat O. Macromolecules 2002;35(10):4050–4055.
[23] Buhmann MD. Acta Numerica 2000;9:1–38.
[24] Hosemann R, Bagchi SN. Direct Analysis of Diffraction by Matter. Amsterdam: North-Holland 1962; p. 89.
[25] Bonart R. Kolloid Z u Z Polymere 1966;211:14–33.
[26] Ruland W. Colloid Polym Sci 1977;255(5):417–427.
[27] Ruland W. Colloid Polym Sci 1978;256:932–936.
[28] Stribeck N, Ruland W. J Appl Cryst 1978;11(5):535–539.
[29] Méring J, Tchoubar D. J Appl Cryst 1968;1:153–165.
[30] Tchoubar D, Méring J. J Appl Cryst 1969;2:128–138.
[31] Schmidt PW. J Math Phys 1967;8:475–477.
[32] Burger C, Ruland W. Acta Cryst 2001;A57:482–491.
[33] Haberäcker P. Digitale Bildverarbeitung. München: Hanser 1989.
[34] Rosenfeld A, Kak AC. Digital Picture Processing, volume 1. London: Academic Press 1982.
[35] Spontak RJ, Williams MC, Agard DA. Polymer 1988; 29:387–395.
[36] Conner WC, Webb SW, Spanne P, Jones KW. Macromolecules 1990;23:4742–4747.